

Theoretical study of kinetic isotope effects on hydrogen abstraction reactions

Yuzuru Kurosaki

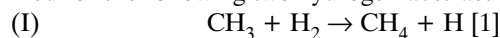
Abstract Effects of isotopic substitutions of “spectator” hydrogens on rate constants have been theoretically examined for the $\text{CH}_3 + \text{H}_2 \rightarrow \text{CH}_4 + \text{H}$ (I) and $\text{C}_2\text{H} + \text{H}_2 \rightarrow \text{C}_2\text{H}_2 + \text{H}$ (II) reactions using variational transition state theory with the multidimensional semiclassical tunneling correction. A small but significant secondary isotope effect was found for reaction (I) but almost no isotope effect was found for reaction (II). This is because the potential energy surface for reaction (II) has an “early” character.

Key words *ab initio* molecular orbital method • hydrogen abstraction reaction • potential energy surface • secondary isotope effect • transition state theory • tunneling

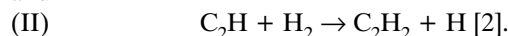
Introduction

Isotope effects (IEs) on chemical reaction rates due to tunneling can be classified as three kinds: primary, secondary, and reaction-path curvature effects. The primary IE originates from the effective mass for the reaction coordinate and is seen when an atom in a bond that is formed or broken is replaced with an isotope. The secondary IE originates from variation in the zero-point energy (ZPE) along the reaction coordinate and is seen when a “spectator” atom is replaced with an isotope. This effect is usually small as compared to the primary IE and often shows an inverse effect, i.e., an isotopic substitution reduces the rate constant. The reaction-path curvature effect originates from the corner cutting of the tunneling path. The curvature of the reaction path depends only on the mass combination of the system; for example, it is large for a heavy-light-heavy system and small for a light-heavy-light system.

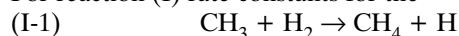
In this work, effects of isotopic substitutions of “spectator” hydrogens on rate constants have been theoretically examined for the following two hydrogen abstraction reactions:



and



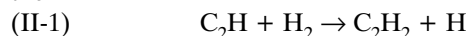
For reaction (I) rate constants for the



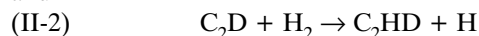
and



reactions were calculated and for reaction (II) those for the



and



were compared over a wide temperature range. Note that reaction rate constants for reactions (I-1) and (I-2) were

Y. Kurosaki
Advanced Photon Research Center,
Japan Atomic Energy Research Institute,
Umemidai, Kizu-cho, Soraku-gun, Kyoto 619-0215, Japan,
Tel.: +81 77/ 471 3400, Fax: +81 77/ 471 3316,
e-mail: kurosaki@apr.jaeri.go.jp

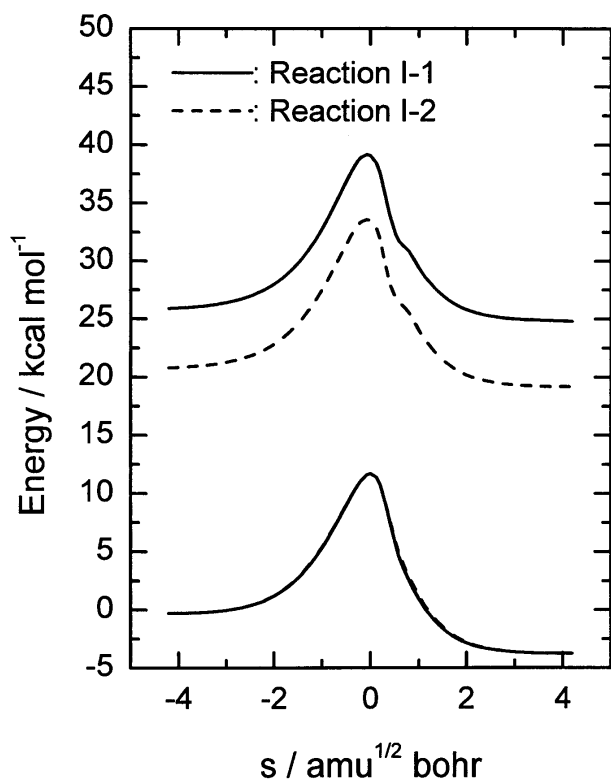


Fig. 1. Electronic and VAG potential curves along IRC for reactions (I-1) and (I-2).

recently measured at 5 K [3], although these measurements were done for solid-phase reactions, i.e., the $\text{CH}_3 + \text{H}_2$ and $\text{CD}_3 + \text{H}_2$ reactions in solid $p\text{-H}_2$, but not for gas-phase reactions.

Methods of calculation

Geometry optimizations were done at the second-order Møller-Plesset perturbation level of theory (MP2(full)) with the cc-pVTZ basis set. Harmonic vibrational frequencies were calculated analytically at the same level of theory and the optimized geometries were characterized as potential minima or saddle points. Single-point energies for the MP2(full)/cc-pVTZ geometries were obtained at the quadratic configuration interaction level including single and double substitutions and perturbative triple substitutions (QCISD(T,full)) using the cc-pVTZ basis set. Intrinsic reaction coordinates (IRCs) for reactions (I) and (II) were determined at the MP2(full)/cc-pVTZ level. Single-point QCISD(T,full)/cc-pVTZ energies were also calculated at many points on the IRCs. Harmonic vibrational frequencies of generalized normal modes orthogonal to the IRCs were computed at the same points on the IRCs. Thus the vibrationally adiabatic ground-state (VAG) potential energy curves were obtained by adding ZPEs of the generalized harmonic vibrational modes to the QCISD(T,full)/cc-pVTZ energies along the IRCs.

Thermal rate constants were calculated using variational transition-state theory (VTST) with the multidimensional semiclassical tunneling correction. The transmission coefficient was estimated for the calculated VAG potential curves under the centrifugal-dominant small curvature semiclassical adiabatic ground-state (CD-SCSAG) approximation.

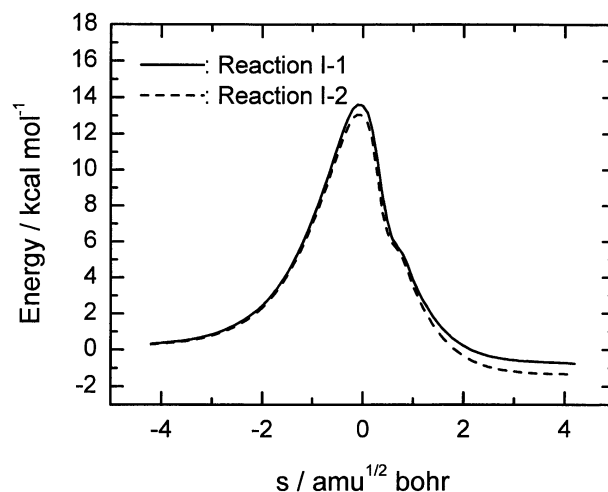
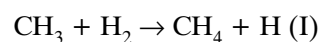


Fig. 2. VAG potential curves along IRC for reactions (I-1) and (I-2).

Results and discussion



Electronic and VAG potential curves along IRC for reactions (1) and (2) are shown in Figure 1. The absolute value of s is the arc length in the unit of $\text{amu}^{1/2} \text{ bohr}$ along IRC from the TS, and the reactants ($\text{CH}_3 + \text{H}_2$) and products ($\text{CH}_4 + \text{H}$) are located in the $s < 0.0$ and $s > 0.0$ regions, respectively. Almost no difference can be seen in the two electronic potential curves. This means that there is almost no primary IE on these reactions, since the IRC employs a mass-scaled coordinate and includes the effective mass. In Figure 2 are compared the two VAG potential curves. In this Figure both the two reactants asymptotes are set to be the zero point of relative energy. It is seen that both the barrier height and barrier width of VAG for reaction (2) are slightly smaller than those for reaction (1). Therefore tun-

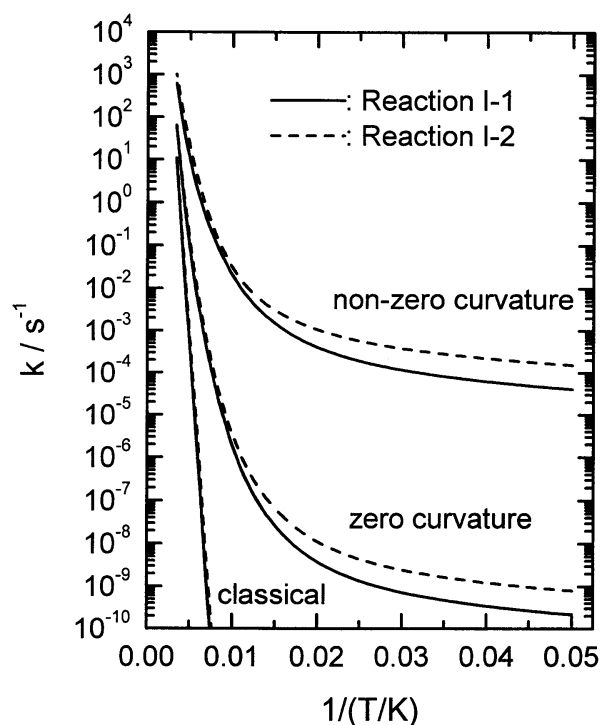


Fig. 3. Calculated rate constants for reactions (I-1) and (I-2).

Table 1. Theoretical and experimental rate constants at 5 K.

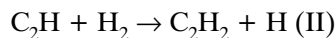
	Theory ^a	Experiment ^b
$\text{CH}_3 + \text{H}_2 \rightarrow \text{CH}_4 + \text{H}$ (I-1)	5.0E-6	~ 0
$\text{CD}_3 + \text{H}_2 \rightarrow \text{CD}_3\text{H} + \text{H}$ (I-2)	2.4E-5	$(4.7+0.5)\text{E-6}$
$k(2)/k(1)$	4.8	$\sim \infty$

^a Present work.^b Taken from Ref. [1].

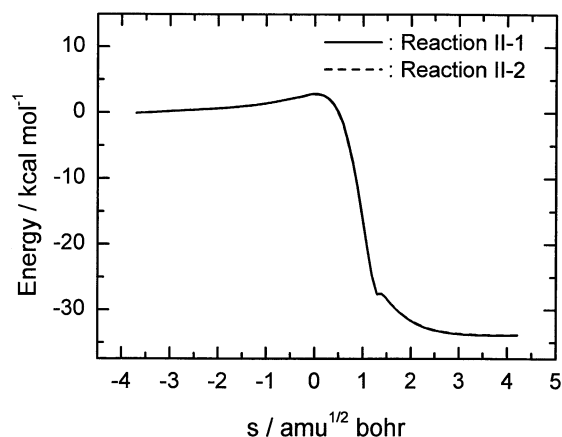
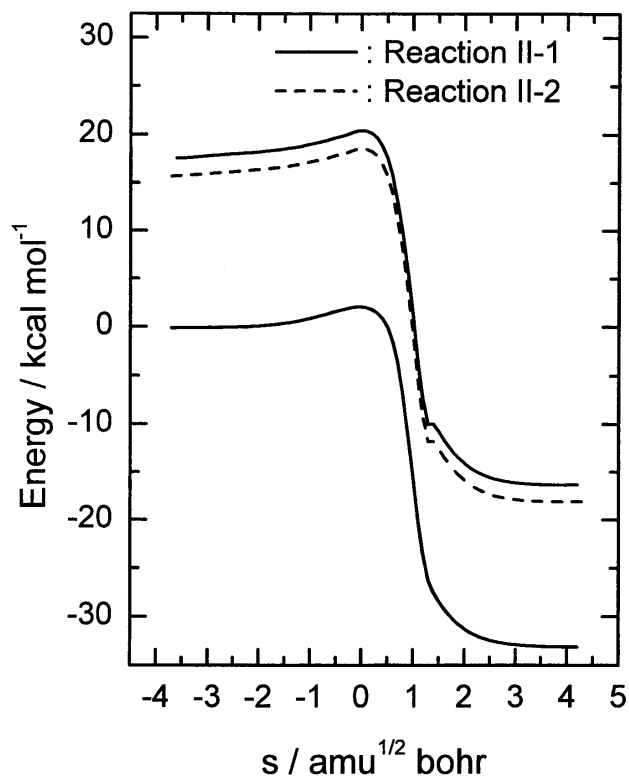
neling probability for reaction (2) is expected to be larger than that for reaction (1) at a given total energy that is smaller than the maximum of the VAG potential.

We consider that unimolecular decomposition of a van der Waals complex produced in the reactant region is a suitable model for reaction (I) in the solid phase. Figure 3 displays Arrhenius plots of unimolecular rate constants for reactions (1) and (2). Rate constants predicted with the three kinds of approximations are given: rate constants without tunneling, with tunneling neglecting curvature, and with tunneling including curvature. Although the absolute amount of the curvature effect is seen to be large, it does not significantly affect the difference between rate constants for reactions (1) and (2). At low temperatures a significant difference is seen between rate constants for reactions (1) and (2); the rate constant for reaction (1) has been calculated to be about 5 times larger than that for reaction (2). One thus conclusively states that difference between the rate constants at low temperatures is caused almost only by the secondary IE.

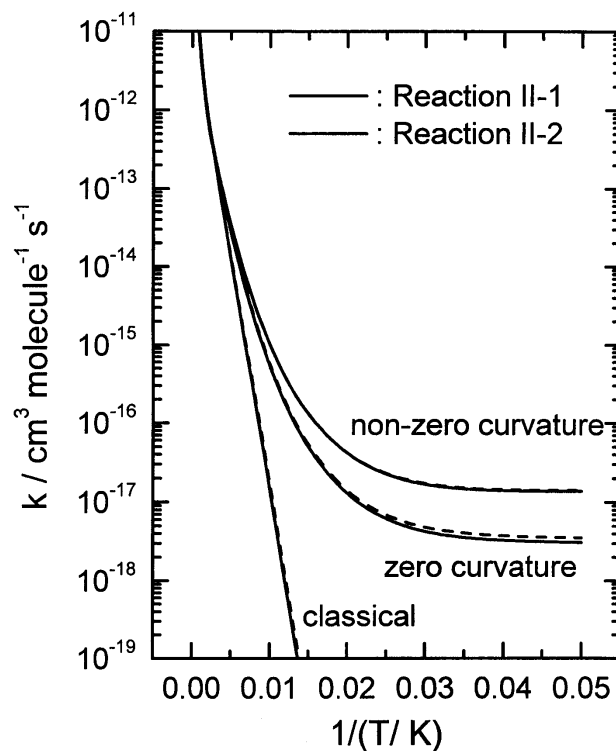
In Table 1 are compared the experimental values [3] with the rate constants calculated with the tunneling correction including the curvature effect. One sees that theory qualitatively agrees but quantitatively disagrees with experiment. This is because the experimental data were measured for solid-phase reactions; CH_3 (CD_3) radicals were produced with the UV photolysis of CH_3I (CD_3I) in solid *p*- H_2 at 5 K and then infrared absorptions of the $\text{CH}_3\text{I}/p\text{-H}_2$ and $\text{CD}_3\text{I}/p\text{-H}_2$ systems were measured after standing in the dark.



Electronic and VAG potential curves along IRC for reactions (1) and (2) are shown in Figure 4, where the TS is located at $s = 0$, the reactants ($\text{C}_2\text{H} + \text{H}_2$) and products

**Fig. 5.** VAG potential curves along IRC for reactions (II-1) and (II-2).**Fig. 4.** Electronic and VAG potential curves along IRC for reactions (II-1) and (II-2).

($\text{C}_2\text{H}_2 + \text{H}$) are located in the $s < 0.0$ and $s > 0.0$ regions, respectively. Almost no difference can be seen in the two electronic potential curves. This means that there is almost no primary IE on these reactions. In Figure 5 are compared the two VAG potential curves. Again, almost no difference can be seen in the two VAG potential curves. Therefore tunneling probability for these reactions are expected to be about the same.

**Fig. 6.** Calculated rate constants for reactions (II-1) and (II-2).

In Figure 6 are displayed Arrhenius plots of bimolecular rate constants for reactions (1) and (2). Rate constants predicted with the three kinds of approximations are given. The absolute amount of the curvature effect is seen to be small as compared to the case of reaction (I) and it causes almost no difference between the rate constants for reactions (1) and (2). Even at low temperatures a significant difference cannot be seen between these rate constants. The reason for no IE on reactions (1) and (2) is considered to be the “early” character of the potential energy surface for reaction (II). “Early” character means that the TS for the reaction is located closer to reactants than products and the barrier height is small, which can be seen from Figures 4 and 5. In this case remarkable changes in vibrational frequencies of the generalized normal modes and reaction-path curvature occur in a region dislocated from the TS. Therefore no IE on reaction (II) can be expected when a spectator H is replaced with D.

Conclusion

In this work effects of isotopic substitutions of “spectator” hydrogens on rate constants have been theoretically examined for the $\text{CH}_3 + \text{H}_2 \rightarrow \text{CH}_4 + \text{H}$ (I) and

$\text{C}_2\text{H} + \text{H}_2 \rightarrow \text{C}_2\text{H}_2 + \text{H}$ (II) reactions using VTST with the multidimensional semiclassical tunneling correction. A small but significant secondary IE was found for reaction (I) and the calculated rate constants for isotopically unsubstituted and substituted reactions of reaction (I) were found to qualitatively agree with experiment. On the other hand, almost no IE was found for reaction (II). This is because the potential energy surface for reaction (II) has an “early” character that dislocates the region of dynamical behavior from the TS.

References

1. Kurosaki Y, Takayanagi T (1999) Theoretical study of an isotope effect on rate constants for $\text{CH}_3 + \text{H}_2 \rightarrow \text{CH}_4 + \text{H}$ and $\text{CD}_3 + \text{H}_2 \rightarrow \text{CD}_3\text{H} + \text{H}$ reactions using variational transition state theory and the multidimensional semiclassical tunneling method. *J Chem Phys* 110:10830–10842
2. Kurosaki Y, Takayanagi T (2000) Theoretical study of kinetic isotope effects on rate constants for the $\text{C}_2\text{H} + \text{H}_2 \rightarrow \text{C}_2\text{H}_2 + \text{H}$ reaction and its isotopic variants. *J Chem Phys* 113:4060–4072
3. Momose T, Hoshina H, Sogoshi N, Katsuki H, Wakabayashi T, Shida T (1998) Tunneling chemical reactions in solid parahydrogen: A case of $\text{CD}_3 + \text{H}_2 \rightarrow \text{CD}_3\text{H} + \text{H}$ at 5 K. *J Chem Phys* 108:7334–7338